Theoretical and numerical studies on a planar gyrotron with transverse energy extraction

Chen Zai-Gao(陈再高)[a)b)], Wang Jian-Guo(王建国)[a)b)†], and Wang Yue(王 玥)[b)]

[a)] *Key Laboratory for Physical Electronics and Devices of the Ministry of Education, Xi'an Jiaotong University, Xi'an* 710049, *China*
[b)] *Northwest Institute of Nuclear Technology, Xi'an* 710024, *China*

(Received 24 December 2013; revised manuscript received 26 April 2014; published online 20 August 2014)

In this paper, we study the planar gyrotron theoretically and numerically. Applying the large-signal theory to the planar gyrotron, the wave equation of electric field and the equation of motion of an electron are simultaneously solved to obtain some characteristic parameters, such as the phase-space plot of electrons, working frequency, startup time, electronic efficiency, and output power of the device. To verify the formulations used in this paper, three-dimensional particle simulations are performed on the same device, and the numerical results accord well with those obtained by using the large-signal theory. Theoretical and numerical results show that the electronic efficiency can reach 21% for the prototype of the planar gyrotron working at the frequency of 0.81 THz.

Keywords: planar gyrotron, terahertz, large-signal theory, particle simulation

PACS: 84.40.Fe, 45.10.Db, 52.65.–y **DOI:** 10.1088/1674-1056/23/10/108401

1. Introduction

Recently, high power terahertz waves are pressingly demanded for widespread applications in imaging, radar, high-data-rate communications, plasma heating and diagnostics, and medical research, etc.[1–4] These applications require higher power, more reliable THz radiation sources. The vacuum electron device has the merit of high power output and relatively compact structure, so many publications are concerned with vacuum electronic terahertz devices, such as the gyrotron, backward wave oscillator (BWO), surface wave oscillator (SWO), free electron laser, and folded-waveguide TWT.[5–11] Among these devices, the gyrotron is one of the most promising sources in the subterahertz band of 0.1 THz–1.0 THz. To improve the electron efficiency and raise the output power of the gyrotron, Ginzburg *et al*. suggested using a planar scheme with a sheet electron beam and transverse (with respect to the electron's translation velocity) electromagnetic energy extraction instead of the conventional cylindrical configuration.[11] The main advantage of the new structure is to ensure coherent radiation from a large-size sheet electron beam, which is due to effective mode selection over the open transverse coordinate and synchronization of radiation from different beam fractions by transverse electromagnetic energy fluxes.

The working characteristics of the planar gyrotron depend on many parameters, such as the shape and sizes of the geometric structure, parameters of the sheet electron beam, and the guiding magnetic field, etc. To further study its working characteristics, the large-signal theory and particle simulation code are used for the same prototype of a planar gyrotron. The theoretical and numerical results presented in this paper agree well with each other.

The rest of this paper is organized as follows. In Section 2, the theoretical model of a planar gyrotron is briefly introduced by using the large-signal theory, and theoretical results are presented for a prototype of the planar gyrotron. The three-dimensional (3D) particle-in-cell (PIC) simulation results of the proposed planar gyrotron are presented in Section 3. Conclusions are made in Section 4.

2. Theoretical model and results

The basic geometric model of the planar gyrotron is shown in Fig. 1. The electrons move in the electromagnetic field, and they follow the Newton–Lorentz equation,

$$\frac{\mathrm{d}}{\mathrm{d}t}(\gamma \boldsymbol{v}) + \eta(\boldsymbol{v} \times \boldsymbol{B}_0) = -\eta(\boldsymbol{E} + \boldsymbol{v} \times \boldsymbol{B}), \tag{1}$$

where $\boldsymbol{v}$ denotes the velocity of the electron, $\boldsymbol{u} = \gamma \boldsymbol{v}$, $\gamma = \left[1 + u^2/c^2\right]^{1/2}$, $\eta = |e|/m_0$, $\boldsymbol{B}_0$ is the external guiding magnetic field along the z direction, $\boldsymbol{E}$ and $\boldsymbol{B}$ are the electric and magnetic fields generated by the rotating electrons, whose moving trajectory is shown in Fig. 2.

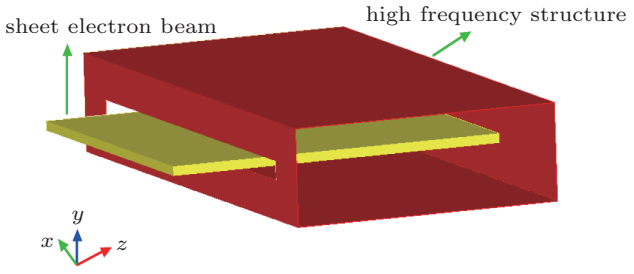


Fig. 1. (color online) Geometric model of the planar gyrotron.

†Corresponding author. E-mail: wanguiuc@mail.xjtu.edu.cn

© 2014 Chinese Physical Society and IOP Publishing Ltd

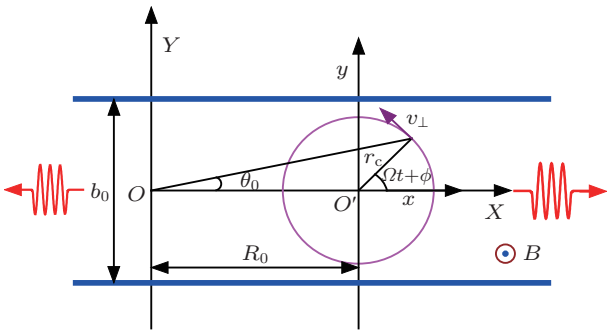


Fig. 2. (color online) Projection of electron orbit in the planar gyrotron.

The wave equation of the electric field is described as

$$\nabla^2 \boldsymbol{E} - \frac{1}{c^2}\frac{\partial^2 \boldsymbol{E}}{\partial t^2} = \mu_0 \frac{\partial \boldsymbol{J}}{\partial t}, \tag{2}$$

where the electric current and its Fourier transform are, respectively,

$$J_\omega(r,t) = J_\omega(r)\exp(\mathrm{i}\omega t), \tag{3a}$$

$$j_\omega(r) = 1/2\pi \int_0^\infty (J(r,t)\exp(-\mathrm{i}\omega t)). \tag{3b}$$

According to the configuration of the geometric structure and the electron beam in the planar gyrotron, there exists the electric field only in the x direction, which satisfies

$$\boldsymbol{E} = \boldsymbol{x} Re\left(A(x,z,t)\sin(\pi s y/b_0)\exp(\mathrm{i}\omega t)\right), \tag{4}$$

where the angular frequency is expressed as

$$\omega = \sqrt{\omega_{c0}^2 + (\pi n c/l_z)^2}. \tag{5}$$

In Eqs. (4) and (5), $\omega_{c0} = \pi s c/b_0$, b_0 is the space gap between the top and bottom plates, l_z is the length in the z direction, s and n are the numbers of the mode variations in the y and z directions, and c is the speed of light in vacuum.

The angular frequency (5) is different from that given in Ref. [11], where it is valid only for the case of $n = 1$. Here we extend the angular frequency for any value of n.

By multiplying both sides of Eq. (2) by the conjugate of $e_s = \sin(\pi s y/b_0)\exp(\mathrm{i}\omega_{c0}t)$, and using Eq. (4) and integrating it by y, we obtain

$$\frac{\partial^2 A}{\partial x^2} - \mathrm{i}\mu_0\omega\sigma A - 2\mathrm{i}\frac{\omega}{c^2}\frac{\partial A}{\partial t} = \frac{2\mu_0 \mathrm{i}\omega\int J\mathrm{e}^{\mathrm{i}\omega t}e_s^* \mathrm{d}y}{b_0}. \tag{6}$$

Define

$$P = \mathrm{i}u_t \exp(-\mathrm{i}\Lambda), \tag{7}$$

where $u_x + \mathrm{i}u_y = \mathrm{i}u_t\exp[\mathrm{i}(\Omega t+\phi)]$, $\Lambda = \omega t - (\Omega t+\phi) + \omega t_0$, and $\Omega = \eta B_0/\gamma_0$.

From Eq. (1), we have

$$\left[\mathrm{d}/\mathrm{d}t + \mathrm{i}\left(\omega - \frac{\Omega_0}{\gamma}\right)\right]P = -\frac{1}{2}\eta A(x,z,t). \tag{8}$$

Defining the dimensionless parameters as follows: $X = \pi\beta_{\perp0}^2 x/\beta_{\|0}\lambda$, $Z = \pi\beta_{\perp0}^2 z/\beta_{\|0}\lambda$, $\tau = \omega t\beta_{\perp0}^4/8\beta_{\|0}^2$, $\sigma_{\mathrm{norm}} = \mu_0\omega\sigma\beta_{\|0}^2\lambda^2/\pi^2\beta_{\perp0}^4$, and $a = eA/(m\omega c\beta_{\perp0}^3\gamma_0)$, and expanding the field magnitude in Fourier series,

$$a = \sum_{n=1}^{\infty} a_n(X,\tau)\sin\frac{n\pi}{L_z}Z,$$

we have the following expression from Eq. (6)

$$\begin{aligned}&\mathrm{i}\frac{\partial^2 a_n}{\partial X^2} + \sigma_{\mathrm{norm}}a_n + \frac{\partial a_n}{\partial \tau}\\ &= \frac{1}{L_Z}\left[2\mu_0 Je\lambda^2\beta_{\|0}/\pi^2\beta_{\perp0}^6 mc\gamma_0 b_0\right]\\ &\times\int_0^{L_Z}\frac{1}{\pi}\int qd\theta\sin\frac{n\pi}{L_Z}Z\mathrm{d}Z.\end{aligned} \tag{9}$$

Defining

$$q = \frac{P}{|P^{(0)}|}, \tag{10}$$

we obtain the equation of motion from Eq. (8) as

$$\frac{\partial q}{\partial Z} + \mathrm{i}q\left(-1+|q|^2\right) = -\sum_{n=1}^{\infty} a_n(X,\tau)\sin\frac{n\pi}{L_Z}Z, \tag{11}$$

where the normalized detuning is

$$\Delta = \frac{2}{\beta_{\perp0}^2}\left(1 - \frac{\Omega_0}{\gamma_0\omega}\right), \tag{12}$$

with Δ being a very important parameter to solve Eq. (11) , it is different from that given in Ref. [11], but exactly the same as Eq. (4.49b) presented in Ref. [12].

We use the Crank–Nicholson finite-difference method to solve Eq. (6).[13,14] To do so, the dimensionless variable X is uniformly discretized into M segments, ΔX and $\Delta\tau$ denote respectively the spatial increment of X and the time step of τ, N and m in $(a_n)_m^N$ are the indices of X and τ. The radiation boundary condition at $X = 0$ is described as

$$\begin{aligned}&\left(1 + \frac{1}{\sqrt{\mathrm{i}\pi}}\frac{1}{X}2\sqrt{\tau}\right)(a_n)_0^N\\ &= \frac{1}{\sqrt{\mathrm{i}\pi}}\frac{1}{X}2\sqrt{\tau}(a_n)_1^N + \frac{1}{\sqrt{\mathrm{i}\pi}}\frac{1}{X}\\ &\times\sum_{k=1}^{N-1}\left((a_n)_1^{N-k} - (a_n)_0^{N-k}\right)\cdot 2\sqrt{\tau}\left(\sqrt{k+1} - \sqrt{k}\right).\end{aligned} \tag{13}$$

The radiation boundary condition at $X = L_X$ is described as

$$\begin{aligned}&\left(1 + \frac{1}{\sqrt{\mathrm{i}\pi}}\frac{1}{\Delta X}2\sqrt{\Delta\tau}\right)(a_n)_M^N\\ &= \frac{1}{\sqrt{\mathrm{i}\pi}}\frac{1}{\mathrm{d}X}2\sqrt{\Delta\tau}(a_n)_{M-1}^N - \frac{1}{\sqrt{\mathrm{i}\pi}}\frac{1}{\mathrm{d}X}\\ &\times\sum_{k=1}^{N-1}\left((a_n)_M^{N-k} - (a_n)_{M-1}^{N-k}\right)\cdot 2\sqrt{\Delta\tau}\left(\sqrt{k+1} - \sqrt{k}\right).\end{aligned} \tag{14}$$

The equation of motion of an electron (11) is solved here by using the fourth order Runge–Kutta method. By solving Eqs. (9) and (11) simultaneously, we can obtain the phase-space distribution of the electrons, the frequency of the generated terahertz signal, the electronic efficiency, etc. Here, we take the parameters listed in Table 1 as a prototype of the planar gyrotron, where the dimensions of the planar structure are 2.4 mm, 0.2 mm, and 3.8 mm in the x, y, and z directions respectively; the planar gyrotron is driven by an electron beam with a beam voltage of 30 kV and a linear current density of 18 A/cm, the pitch ratio α and length of the electron beam are 1.0 and 1.2 mm respectively, and the guiding magnetic field strength is 27.6 T. We solve Eqs. (9) and (11) by sweeping n, and find that the device starts to oscillate when $n = 8$ for the parameters listed in Table 1. Typical results are shown in Figs. 3–5.

Table 1. Parameters of the planar gyrotron with transverse output.

Beam voltage/kV	Linear current density/(A/cm)	Pitch ratio	Length in the x direction/mm	Length in the y direction/mm	Length in the z direction/mm	Magnetic field strength/T
30	18	1.0	2.4	0.2	3.8	27.6

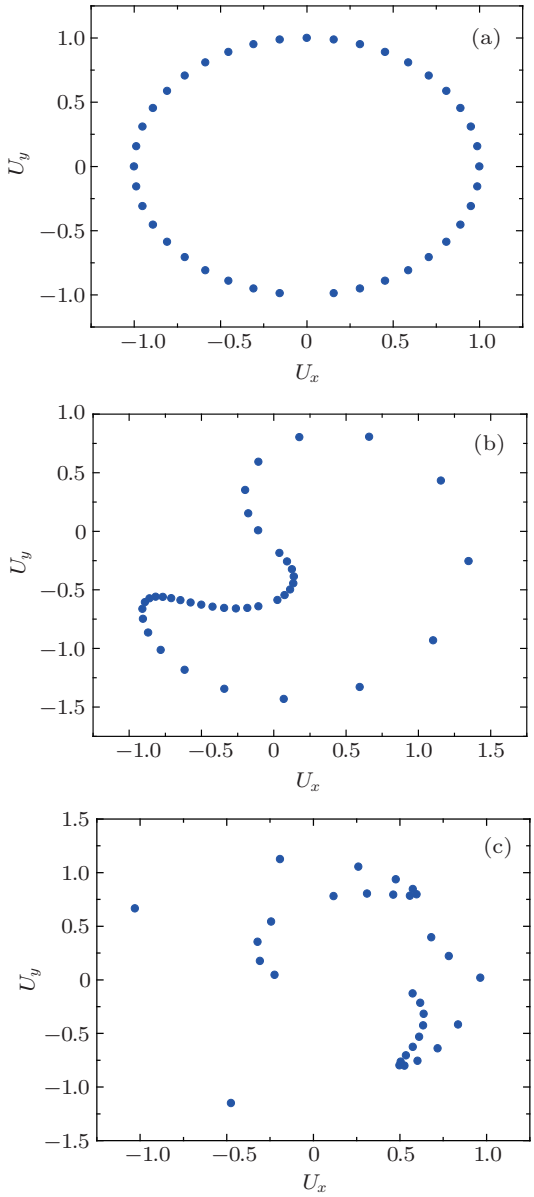


Fig. 3. (color online) Phase-space of electrons at different positions at $t = 100$ ns for (a) $(L_X/2, 0, 0)$, (b) $(L_X/2, 0, L_Z/2)$, (c) $(L_X/2, 0, L_Z)$.

Figure 3 shows the phase-space distribution of electrons at 100 ns at different positions on the line of $X = L_X/2$ and $y = 0$. At point $(L_X/2, 0, 0)$, the electrons enter into the interaction space, the distribution of the electrons in the phase-space is uniform as shown in Fig. 3(a). At the point $(L_X/2, 0, L_Z/2)$, the electrons are modulated to some extent. At point $(L_X/2, 0, L_Z)$, the electrons are bunched significantly.

Figure 4(a) shows the variation of $\mathrm{Re}(a_n)$ with time and its fast Fourier transform (FFT). It can be seen from Fig. 4(b) that the corresponding frequency is 0.8008 GHz, which implies that $A(x, z, t)$ is a slowly varying function, and hence, the frequency of the generated electromagnetic wave is dominated by ω. Substituting $n = 8$ into Eq. (5), we obtain the working frequency of the planar gyrotron to be $f_{\mathrm{work}} = 0.814$ THz.

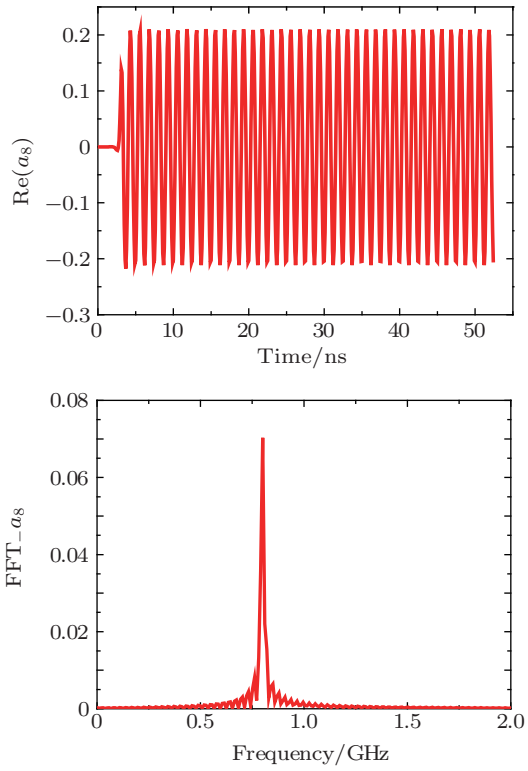


Fig. 4. (color online) $\mathrm{Re}(a_n)$ and its Fourier transform.

The transverse conversion efficiency from the electron beam to the terahertz signal is defined as $\eta_\perp = 1 - (1/2\pi L_X)\int_0^{L_X}\int_0^{2\pi}|q|^2\,\mathrm{d}\theta_0\,\mathrm{d}X$, the total efficiency $\eta_{\text{total}} = \eta_\perp\alpha^2/(1+\alpha^2)$, which is plotted in Fig. 5. It can be seen that the planar gyrotron starts to rise up very fast in about 2 ns, and the total conversion efficiency is 0.2069, so the output power is $W_{\text{out}} = 4G\eta_\perp L_X$=13.4 kW.

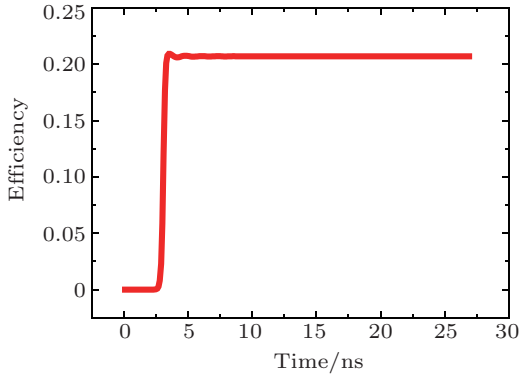


Fig. 5. (color online) Conversion efficiency versus time.

The power of the electromagnetic wave is

$$W_{\text{EM}} = 2\sum_{n=1}^{\infty}\text{Im}\left(\frac{\partial a_n^*}{\partial X}\cdot a_n\Big|_{X=L_X} + \frac{\partial a_n}{\partial X}\cdot a_n^*\Big|_{X=0}\right)\cdot L_Z.$$

When the device works in a steady state, W_{EM} should be very close to W_{out}. To verify the formulations used in this paper, we define the relative error as $\text{err} = 10\log|(W_{\text{out}} - W_{\text{EM}})/W_{\text{out}}|$, and plot it in Fig. 6; we can see that the relative error is about -25 dB.

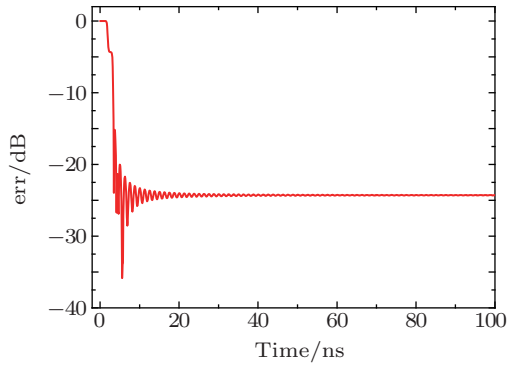


Fig. 6. (color online) Relative error versus time.

3. Particle simulation and results

According to the configurations of geometric structure and electron beam shown in Fig. 1, the simulation of the planar gyrotron should be performed by using the 3D code.[15–17] To further verify the formulations used in this paper, we use the 3D parallel fully electromagnetic particle simulation code UNIPIC-3D[18] to simulate the planar gyrotron. UNIPIC-3D is the 3D version of the 2.5-dimensional code UNIPIC,[19–21] which has been used to simulate the high power surface wave oscillator in the subterahertz band.[7,22–26]

Typical numerical results are given in Figs. 7–10. Figure 7 displays the 3D distribution of the electric field E_x at 4.0 ns. It can be seen that a steady-state mode of the electric field is formed with 8 variations along the z direction, which demonstrates that the device can work for the $n = 8$ case.

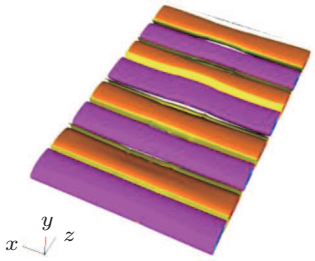


Fig. 7. (color online) 3D distribution of E_x.

Figures 8(a) and 8(b) are the time history and spectrum of the electric field E_x at the output port of the device, respectively. Figure 8(b) indicates that the working frequency of the device is about 0.813 THz, which accords very well with the result obtained by using the large-signal theory.

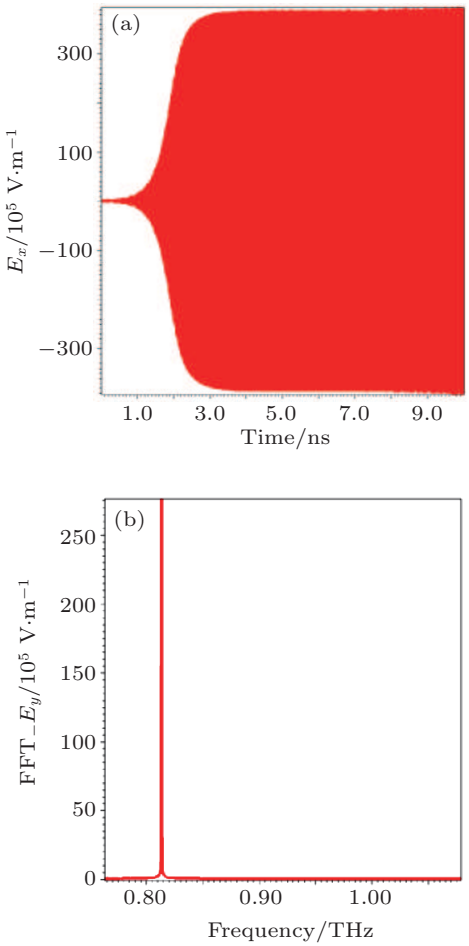


Fig. 8. (color online) (a) Time history and (b) spectrum of electric field E_x at output port of the device.

Figure 9 shows the distributions of electron velocity at different times. At 0.5 ns, the electrons are rotating guided by the external magnetic field, but they are not obviously bunching, so no terahertz signal is generated, which can also be seen from Fig. 8(a). At 10 ns, the electrons are gyrating and bunching significantly, and the terahertz signal is being generated and remains stable.

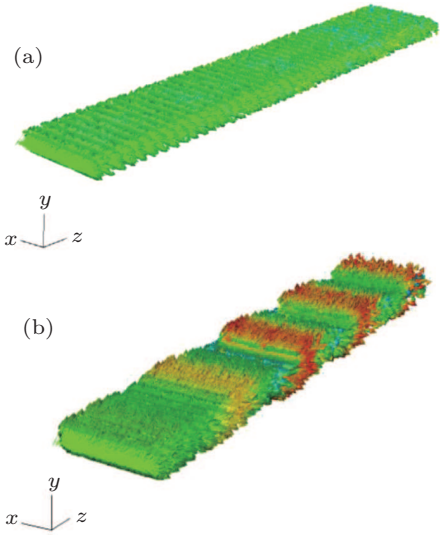


Fig. 9. (color online) Distributions of electron velocity at (a) 0.5 ns and (b) 10 ns.

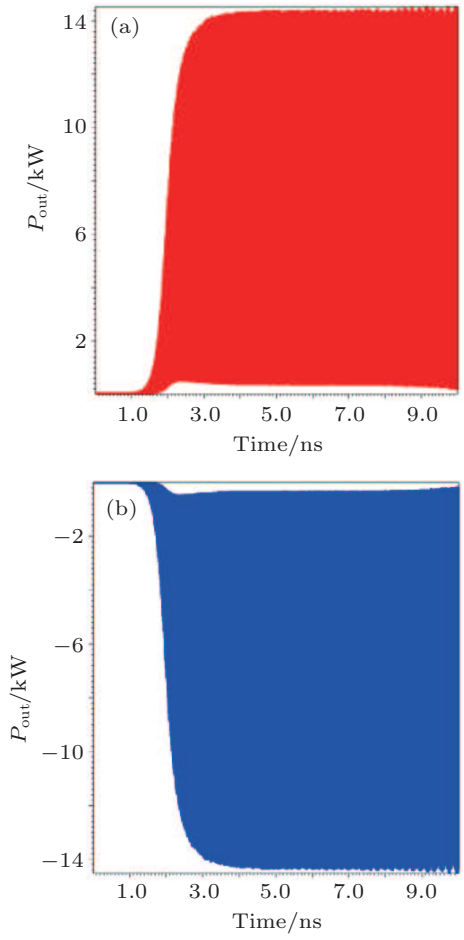


Fig. 10. (color online) Simulated output powers of the planar gyrotron in (a) x and (b) $-x$ directions.

The simulated output power is presented in Fig. 10, where figures 10(a) and 10(b) show respectively the power outputs from the x and $-x$ directions, which are nearly the same in magnitude, but opposite in direction, of power flux. It can be seen from these two figures that the output transient power is about 13.8 kW, the total output average power is also about 13.8 kW, the conversion efficiency of the electron beam to the terahertz wave is about 21%, and the startup time of the device is about 2 ns. These three characteristic parameters accord well with those obtained using the large-signal theory.

4. Conclusions

By solving the wave equation and equation of motion simultaneously for a prototype of a planar gyrotron, some characteristic parameters are provided in this paper for the phase-space plot of electrons, working frequency, startup time, electronic efficiency, and output power of the device.

We use two methods to verify the theory used in this paper. The first one is to compare the lost power of the electron beam with the output power of the generated electromagnetic wave. When the device works at the steady state, they should be very close to each other. The calculated relative error between them is about -25 dB, which indicates that the formulations and computation method are correct. The second method is to use the 3D PIC simulations. The PIC simulation results accord well with those obtained by using the large-signal theory.

Theoretical and numerical results show that the electronic efficiency can reach 21% for the prototype of the planar gyrotron working at a frequency of 0.81 THz. The output power of the generated terahertz signal increases with the width of the electron beam increasing. We obtain $W_{\rm out} = 13.4$ kW for the prototype of the planar gyrotron with $l_x = 1.2$ mm, if we increase the length of the electron beam to 1.2 cm, the output power of the planar gyrotron is expected to be more than a hundred kilowatts.

The working property of the planar gyrotron depends on many parameters, such as the width, height, and length of the device structure, the voltage, current density, width, and position of the electron beam, the external magnetic field, etc. Next, we wish to optimize the parameters of the planar gyrotron by using the large-signal theory, particle simulation, and genetic algorithms, which have been used to optimize the relativistic backward wave oscillator.[27]

References

[1] Siegel P H 2002 *IEEE Trans. Microwave Theory Technol.* **50** 910
[2] Booske J H, Dobbs R J, Joye C D, Kory C L, Neil G R, Park G, Park J and Temkin R J 2011 *IEEE Trans. Terahertz Sci. Technol.* **1** 54
[3] Zhang T Y and Cao J C 2004 *Chin. Phys.* **13** 1742
[4] Chen Z and Cao J C 2013 *Chin. Phys. B* **22** 059201
[5] Glyavin M Y, Luchinin A G and Golubiatnikov G Y 2008 *Phys. Rev. Lett.* **100** 015101

[6] Bratman V, Glyavin M, Idehara T, Kalynov Y, Luchinin A, Manuilov V, Mitsudo S, Ogawa I, Saito T, Tatematsu Y and Zapevalov V 2009 *IEEE Trans. Plasma Sci.* **37** 36
[7] Wang G, Wang J, Tong C, Li X, Wang X, Li S and Lu X 2013 *Phys. Plasmas* **20** 043105
[8] Carr G L, Martin M C, McKinney W R, Jordan K, Neil G R and Williams G P 2002 *Nature* **420** 153
[9] Shin Y M, Baig A, Barnett L R, Luhmann N C, Pasour J and Larsen P 2011 *IEEE Trans. Electron. Dev.* **58** 3213
[10] Gong Y, Yin H, Yue L, Lu Z, Wei Y, Feng J, Duan Z and Xu X 2011 *IEEE Trans. Plasma Sci.* **39** 847
[11] Ginzburg N S, Zotova I V, Sergeev A S, Zaslavsky V Y and Zheleznov I V 2012 *Phys. Rev. Lett.* **108** 105101
[12] Kartikeyan M V, Borie E, Thumm M K A 2004 *Gyrotron: High Power Microwave and Millimeter Wave Technology* (Berlin/Heidelberg: Springer-Verlag)
[13] Sun G and Trueman C W 2003 *Electron. Lett.* **39** 595
[14] Chen J and Wang J 2009 *IEEE Trans. Anten. Propag.* **57** 3375
[15] Shin Y M, Baig A, Barnett L R, Tsai W C and Luhmann N C 2012 *IEEE Trans. Electron. Dev.* **59** 234
[16] Shi Z, Gamzina D, Barnett L R, Baig A and Luhmann N C 2013 *IEEE Trans. Electron. Dev.* **60** 2912
[17] Chen Z, Wang J, Wang Y, Qiao H, Guo W and Zhang D 2014 *Chin. Phys. B* **23** 068402.
[18] Wang J, Chen Z, Wang Y, Zhang D, Liu C, Li Y, Wang H, Qiao H, Fu M and Yuan Y 2010 *Phys. Plasmas* **17** 073107
[19] Wang J, Zhang D, Liu C, Li Y, Wang Y, Wang H, Qiao H and Li X 2009 *Phys. Plasmas* **16** 033108
[20] Wang J, Wang Y and Zhang D 2006 *IEEE Trans. Plasma Sci.* **34** 681
[21] Wang J G 2013 *Mod. Appl. Phys.* **4** 251 (in Chinese)
[22] Zhang H, Wang J, Tong C, Li X and Wang G 2009 *Phys. Plasmas* **16** 123104
[23] Li X, Wang J, Song Z, Chen C, Sun J, Zhang X and Zhang Y 2012 *Phys. Plasmas* **19** 083111
[24] Wang G, Wang J, Li S, Wang X, Tong C and Lu X 2013 *Acta Phys. Sin.* **62** 150701 (in Chinese)
[25] Li S, Wang J, Tong C, Wang G, Lu X and Wang X 2013 *Acta Phys. Sin.* **62** 120703 (in Chinese)
[26] Li X Z, Wang J G, Sun J, Song Z M, Ye H, Zhang Y C, Zhang L J and Zhang L G 2013 *IEEE Trans. Electron. Dev.* **60** 2931
[27] Chen Z, Wang J, Wang Y, Qiao H, Zhang D and Guo W 2013 *Phys. Plasmas* **20** 113103